Preliminary Design and Assessment of a Waste Heat Recovery System for a Hybrid-Electric Heavy-Duty Vehicle

Teresa Donateo[1*], Gabriele Marti[1], Talha Mujahid[1], Francesco Nuzzo[1], Simone Tundo[1], Lorenzo Zezza[1]

Angelo Algieri[,2] Pietropaolo Morrone[,2]

[1] Department of Engineering for Innovation, University of Salento, Lecce, Italy
[2] Department of Mechanical Engineering, Energy Engineering and Management, University of Calabria, Arcavacata di Rende (CS), Italy

[*]E-mail: teresa.donateo@unisalento.it

Abstract. Heavy-duty vehicles (HDVs) are major contributors to greenhouse gas emissions and urban air pollution, particularly during cold-start and transient conditions where fuel efficiency and exhaust aftertreatment systems are less effective. This study proposes a novel waste heat recovery (WHR) architecture integrated into a hybrid HDV powertrain to address these challenges. The system combines an Organic Rankine Cycle (ORC) and a parallel hybrid electric powertrain. A quasi-static simulation model is developed, incorporating validated sub-models for the Internal Combustion Engine (ICE), electric propulsion system, battery, and WHR unit. The model is parameterized and preliminarily validated using a publicly available dataset from a 6-cylinder turbocharged Isuzu FTR 850 truck equipped with a Euro III 7.79-liter diesel engine, recorded under real-world driving conditions in South Africa across 28 trips and three payload configurations (0 kg, 1500 kg, and 3000 kg). The dataset includes key variables such as engine speed, exhaust temperature, fuel flow rate, and coolant temperature, enabling the assessment of cold-start dynamics and thermal recovery potential. The simulation examines energy fluxes from the exhaust and coolant circuits and explores the synergies between hybrid energy management and WHR. The results indicate that the proposed system can reduce fuel consumption and improve exhaust thermal profiles. Fuel consumption savings are strongly affected by energy management, ranging from 15% with a simplistic constant power strategy to 32% with the adoption of a fuzzy logic-based control strategy. These findings support the feasibility of WHR–TES hybrid integration in HDVs and offer promising directions for compliance with future emission standards such as Euro VII, EPA 2027, and China VII standards.

1. Introduction

Although HDVs, such as trucks and buses, represent less than 8% of the global vehicle fleet, they are responsible for over 35% of road transport CO_2 emissions [1]. In regions such as Europe, China, and the United States, HDVs disproportionately contribute to Green House Gases (GHGs)

and air pollutants compared to their numbers. For example, medium and heavy-duty vehicles constitute only about 5% of U.S. vehicles but produce roughly 23–24% of transportation GHG emissions; and contribute on the order of 40–60% of on-road nitrogen oxides (NO_x) and particulate matter (PM) [2]. This disproportionate impact has made emissions from HDVs a critical target for both global and regional climate and air quality initiatives.

Environmental regulators have steadily tightened HDV emission standards over the past decade. The Euro VI standard (in effect since 2013) mandated advanced aftertreatment systems, dramatically reducing allowable NO_x and PM. However, real-world tests revealed challenges in controlling emissions during cold-start and low-load operations, when exhaust aftertreatment is least effective [3]. In response, upcoming Euro VII regulations are being formulated with even stricter limits, including dedicated provisions for cold-start emissions and urban driving conditions [4]. Similarly, China's Stage VI standards (China VI, implemented from 2019 to 2021) introduced a World Harmonized Transient Cycle (WHTC) test that explicitly includes a cold-start segment (approximately 14% of the cycle), reflecting the importance of startup emissions. China's next-stage rules (China VII) are expected to further tighten NO_x limits, particularly under cold-start and low-speed, low-load conditions [5-6]. In the United States, the Environmental Protection Agency's latest heavy-duty rules (EPA 2027) mandate a roughly 82% reduction in NO_x emissions compared to previous standards, extending stringent control to longer operating periods, including idle and cold-start phases [7]. These regulatory trends underscore that future HDV powertrains must drastically reduce emissions under all conditions, especially during engine warm-up, to comply with standards and protect urban air quality.

Meeting these goals is challenging with current diesel engine technology. Even modern heavy-duty diesel engines achieve a brake thermal efficiency of only about 43–46% [8], meaning that well over half of the fuel's energy is lost as waste heat. A substantial portion of the fuel energy (typically 20–30% or more) is lost from the engine in the form of high-temperature exhaust gases [9], with additional energy being dissipated through the coolant and other thermal losses. These inefficiencies not only waste fuel (increasing CO_2 emissions) but also represent an opportunity: If some of this waste heat is recovered and converted to useful work. Indeed, effective recovery of HDV waste heat has been identified as a key strategy for meeting increasingly stringent fuel economy and CO_2 standards [10]. By tapping into the engine's thermal losses, a WHR system can supplement the powertrain, reducing the load on the engine and thereby lowering fuel consumption and emissions.

One of the most promising WHR technologies for mobile applications is the Organic Rankine Cycle (ORC) [11]. This bottoming cycle can feed recovered power back to the drivetrain or to vehicle auxiliaries, effectively converting waste heat into useful energy. Prior studies have demonstrated the technical and economic feasibility of ORC-based WHR systems in HDVs, particularly in improving fuel efficiency and reducing emissions. For instance, Li et al. [12] analyzed the performance of a subcritical ORC system in a fully loaded heavy-duty truck and reported fuel economy improvements ranging from 4.5% to 7.5% under various driving conditions. Similarly, Zhao et al. [13] conducted simulations using real-life driving cycles from Europe, the U.S., and China finding fuel consumption reductions of 2.5%, 3.1%, and 3.4%, respectively, depending on the region-specific cycle characteristics. Thantla et al. [14] explored a dual-loop ORC configuration and found that it not only enhanced thermal efficiency but also provided better adaptability to dynamic engine load conditions, a critical feature for real-world operations. Another article by Wang et al. [15] highlighted the inefficiencies of internal combustion engines, where gasoline engines convert only 20-30% of fuel energy into useful

power, while diesel engines achieve 30-40% efficiency. This results in substantial energy loss, with 40-45% of energy lost as exhaust heat. The ORC is presented as a promising solution for waste heat recovery, capable of improving thermal efficiency by up to 3.6% and reducing brake specific fuel consumption (BSFC) by 10 g/kWh when integrated with diesel engines. Moreover, their research underscores the importance of optimizing ORC systems to enhance energy recovery and contribute to environmental sustainability. Complementing these findings, Song et al. [16] evaluated the integration of an ORC system into a heavy-duty truck powertrain and concluded that it effectively harnessed exhaust heat to support both propulsion and auxiliary loads, ultimately improving fuel economy and reducing CO_2 emissions. Consequently, ORC-based WHR has garnered considerable attention as a means to enhance diesel HDV efficiency and reduce emissions [17].

Despite these benefits, the practical implementation of ORC-based WHR in commercial HDVs faces notable limitations. A conventional ORC adds extra components, such as heat exchangers, a working fluid circuit, an expander, a condenser, and a pump, which increase the vehicle's weight and complexity. This added mass can partly offset the efficiency gains by increasing the vehicle's fuel consumption, for example, a review found that ORC components, which increase system weight by about 10%, can measurably deteriorate overall fuel economy [18]. Moreover, the thermal operating profile of a vehicle engine is highly dynamic, including engine load and exhaust heat flow that can fluctuate rapidly with driving conditions, such as accelerations, decelerations, and idle periods. ORC systems generally perform best at steady, high-load conditions and can struggle to respond to abrupt transients. Fast changes in exhaust temperature or flow can lead to inefficient operation or even necessitate bypassing the ORC to prevent component damage [19]. During sudden drop-offs in engine load, a traditional ORC may not ingest enough heat to sustain vaporization, causing the expander power to decrease or the working fluid to condense prematurely. At very low loads or during engine warm-up, exhaust gas temperatures can be below the ORC's minimum operating range, rendering the WHR system inactive precisely when the engine is least efficient. These transient and low-power conditions are common in real drive cycles. Thus, they limit the standalone ORC's effectiveness and highlights the need for solutions to make WHR more robust and responsive.

To address the variability of the heat source, researchers have been exploring thermal energy storage (TES) integrated with the ORC, particularly using phase-change materials (PCMs) as the storage medium [19-20].

Another significant advancement in HDV powertrains is hybridization, which involves combining an ICE with electric drive components and energy storage (batteries) in the vehicle. Hybrid HDVs can recuperate braking energy, enable engine stop-start, and allow the engine to run more optimally by smoothing out demand peaks using the electric motor [21]. This not only reduces fuel consumption but also enables the engine to operate in more efficient regions (with higher loads and temperatures), which in turn produces more recoverable waste heat for the WHR system. In a hybrid powertrain, the ORC-generated power can be converted to electricity and stored in the battery or used directly to assist propulsion, effectively increasing the utilization of recovered energy beyond what a conventional powertrain might allow. Conversely, the hybrid control strategy can be designed to load the engine slightly higher (charging the battery or supplying propulsion) at times when additional waste heat recovery is beneficial and rely on the electric motor in conditions where the engine would be inefficient. Researchers have begun to explore this synergy between hybridization an.d WHR. For instance, Mahmoudzadeh et al. [22] integrated an ORC system into a hybrid electric vehicle (HEV) powertrain, observing significant

reductions in fuel consumption across various driving cycles. Specifically, the ORC-equipped HEV demonstrated fuel consumption reductions of approximately 10% on the FTP-75 cycle, 8% on the NEDC, and 7% on the US06 cycle, compared to the baseline hybrid configuration without ORC integration. These findings underscore the potential of ORC systems to enhance further energy utilization in hybrid vehicles, which are already more efficient than conventional internal combustion engine vehicles. Thus, the combination of hybrid energy management and waste heat recovery holds promise for compounding energy savings: the hybrid system ensures the engine operates efficiently and can absorb ORC output flexibly. In contrast, the ORC/WHR system recovers energy that would otherwise be wasted as heat.

Effective energy management is pivotal for optimizing the performance of hybrid HDVs, especially when integrating complex subsystems such as WHR and TES. Traditional energy management strategies, including rule-based and model predictive control (MPC) methods, often struggle to handle the nonlinearities and uncertainties inherent in hybrid powertrains under dynamic operating conditions. Fuzzy Logic Control (FLC) has emerged as a robust alternative, capable of managing such complexities without requiring precise mathematical models. FLC utilizes a set of intuitive "if-then" rules to make decisions based on inputs like engine load, battery state-of-charge (SOC), and exhaust temperature, enabling real-time adaptation to varying driving scenarios. Recent studies have demonstrated the efficacy of FLC in hybrid vehicle applications. For instance, an FLC-based energy management system for a hybrid fuel cell propulsion system in a passenger vessel showed superior performance in reducing fuel consumption compared to conventional strategies [23]. Another study applied FLC to a fuel cell hybrid electric vehicle, achieving improved energy efficiency and balanced state-of-charge (SOC) levels [24]. Moreover, integrating FLC with hybrid energy storage systems, such as combinations of batteries and supercapacitors, has been shown to enhance energy distribution and prolong battery life [25].

Building upon this state of the art, this study proposes a novel fuzzy-logic-based energy management system tailored for hybrid HDVs equipped with WHR. The proposed system aims to optimize power distribution among the engine, electric motor, and energy storage components, taking into account real-time variables and system constraints. By leveraging the adaptability of FLC, the system is expected to enhance fuel efficiency, reduce emissions, and improve overall vehicle performance across a wide range of operating conditions.

To summarize, this study contributes to the scientific literature by proposing:

- A quasi-static model of a diesel truck validated through experimental data acquired in real-world emission tests.
- A hybrid heavy-duty truck powertrain designed to minimize energy consumption and control the temperature and mass flow rate of the exhaust gases.
- An integrated HDV powertrain concept that brings together waste heat recovery, thermal energy storage, and hybridization in a unified simulation framework.
- A charge-depleting energy management over eight hours of working time for the truck based on fuzzy logic.
- A preliminary quantification of the fuel saving obtained from the synergy of hybridization and heat recovery under real-world driving conditions.

2. Reference vehicles and driving cycles

The heavy-duty truck analyzed in this study is an Isuzu FTR850 (Class 6) equipped with a Euro III 6-cylinder, turbocharged intercooled diesel engine [26]. Key specifications of the vehicle and its powertrain are summarized in Table 1 [27]. Notably, the truck is not fitted with any exhaust

aftertreatment system, reflecting an older emission technology. This particular dataset was selected after a broad review of available open data on medium- and heavy-duty diesel trucks.

Table 1. Relevant specifications of the vehicle.

Vehicle	Isuzu FTR 850	Payload	{0 kg; 1500 kg; 3000 kg}	Displacement	7.79 liters
Gross Vehicle Mass (GVM)	15,500 kg	Engine model	Isuzu 6HK1	Number of Cylinders	6
Gross Combination Mass (GCM)	24,000 kg	Emissions standard	Euro III	Power	210 kW (1900 rpm)
Vehicle mass during tests	10,740 kg	Torque	1080 Nm (1500-1800 rpm)	Fuel consumption (H-series)	0.342 lb/HP-h (208 g/kWh)
Transmission and drive type	Hydraulic controlled	Number of gears forward	6	Gear Ratios (inclusive of final ratio)	{38.9; 24.0, 13.85, 9.0,5.88, 4.24}
Tires	11 R22.5- 16PR (radius 0.52m)				

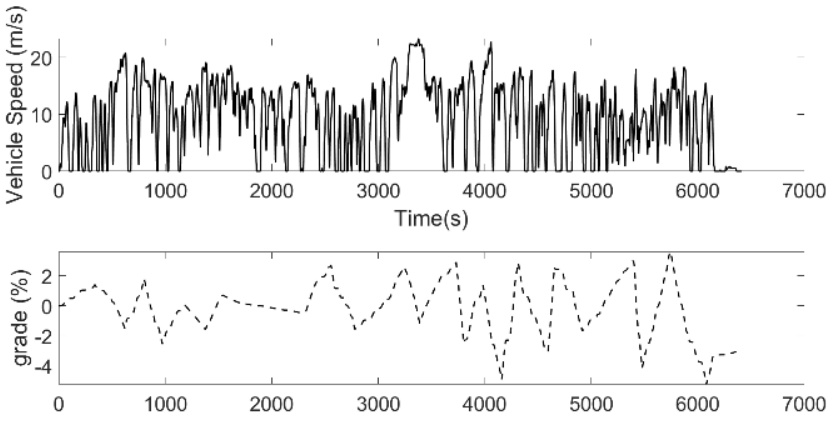

Figure 1. Route and elevation of a real-world trip (trip #4)

Publicly accessible real-world data for such trucks were found to be scarce compared to that for passenger cars or buses. Ultimately, an open dataset from Joubert et al. [26] was chosen, as no suitable data were found for a more modern diesel truck that complies with recent emissions standards. The dataset comprises 28 real-world trips performed with the above vehicle under various payload conditions. The first eight trips were run with the truck unloaded, the next ten trips with a 3,000 kg payload, and the final ten trips with a 1,500 kg payload. All trips follow the same route (approximately 61.7 km, about1.8 hours) in South Africa, driven by the same driver, with identical start and end points at the University of Pretoria's Hatfield campus. An example speed and road grade profile for one of the trips is depicted in Figure 1, showing the highly dynamic driving conditions. During data collection, the truck was equipped with a Portable

Emissions Measurement System (PEMS) connected to the vehicle's OBD-II port and a GPS unit for geospatial data collection. The sampling frequency was 1 Hz for trips 1–8 and 0.2 Hz for trips 11–28. The primary variables recorded from the vehicle (e.g., vehicle speed, engine speed, fuel flow, exhaust emissions) along with their data sources (GPS, OBD-II, PEMS) are summarized in Table 2. A detailed analysis of the dynamics driving conditions recorded in the dataset was performed in a previous investigation [28].

Table 2. List of relevant information from the dataset [26].

Variable	Description	Unit	Source
z	Altitude	m	GPS
T_{amb}	Ambient temperature	°C	PEMS
V	Vehicle speed	km/h	OBD-II
T_{cool}	Coolant temperature	°C	OBD-II
$\dot{m}_{fuel}$	Instantaneous fuel flow	g/s	OBD-II
$\dot{m}_{exh}$	Exhaust mass flow rate	kg/h	PEMS
T_{exh}	Exhaust temperature	°C	PEMS
$\dot{m}_{CO_2}$	Instantaneous mass of CO_2	g/s	PEMS
$\dot{m}_{NO_x}$	Instantaneous mass of NO_x	g/s	PEMS
$\dot{m}_{CO}$	Instantaneous mass of CO	g/s	PEMS

3. Modelling approach

A backward, quasi-static simulation approach was employed to model the vehicle's longitudinal dynamics. The simulation uses a fixed discrete time step, matching the data sampling interval (Δt, typically 1 s), to iterate through each trip's recorded trajectory. For each time step i, the known time histories of vehicle speed $V(i)$ and road grade $\alpha(i)$ serve as inputs, and the required power at the wheels $P_w\ (i)$ is calculated as:

$$\mathrm{P_w\ (i)} = \frac{1}{2}\mathrm{C_d \cdot A_f \cdot \rho_a \cdot\ V(i)^3 + M \cdot g \cdot C_r \cdot V(i) \cdot \cos\alpha(i) + M \cdot g \cdot \sin\alpha(i) \cdot V(i) + M_i \cdot a(i) \cdot V(i)} \quad (1)$$

Where C_d and C_r are the aerodynamic drag and rolling resistance coefficients, respectively, in this study, C_r is assumed to be constant for simplicity (although it can generally vary with speed and tire pressure). M denotes the vehicle mass including curb weight, driver, and payload, and M_i is an effective mass that accounts for the rotational inertial effects of rotating components (often taken as a fraction of $\cong 1.1M$) [29]. $\rho_a(t)$ and A_f are the air density and vehicle frontal area, and $a(i)$ is the vehicle acceleration at time step i. The first term of equation (1) represents the power

lost to aerodynamic drag, the second term corresponds to rolling resistance losses, and the third term represents the power invested in accelerating the vehicle's mass (including a rotational inertia allowance). The key vehicle parameters and constants used in these calculations (drag coefficient, frontal area, etc.) are listed in Table 3.

Table 3. Selection of vehicle parameters.

Parameter	References	Suggested	Selected
C_d	Hammache et al. [30], Arts et al. [31]	0.4-0.7	0.6
C_r	Arts et al. [31]	0.008	0.008
η_{gb}	Vehicle manual	0.96	0.96
P_{aux}	Arts et al. [31]	2-10kW	2 kW

For a conventional powertrain (diesel engine only), the engine must provide not only the wheel power demand but also overcome driveline losses and supply any auxiliary loads. Thus, the instantaneous engine power requirement $P_{eng}(i)$ is computed as:

$$P_{eng}(i) = P_w\,(i)/\eta_{gb} + P_{aux}(i) \quad (2)$$

Where η_{gb} is the efficiency of the drivetrain (gearbox and transmission) and P_{aux} is the parasitic power draw of auxiliary systems (e.g., lighting, radiator fan, coolant pump, etc.).
The backward simulation framework assumes that at each time step the engine can immediately deliver the required power $P_{eng}(i)$ (since fast transient dynamics are not explicitly modelled), which is reasonable under quasi-static conditions. The approach thereby allows estimation of engine operating points (torque and speed) over the drive cycle for use in fuel consumption and emissions calculations.

Deriving an engine fuel consumption map directly from the limited on-road data proved impractical. Instead, a map-based engine model was developed by scaling a reference engine map from the literature. The baseline map was taken from MATLAB/Simulink's built-in Mapped CI Engine model, which represents a modern 1.5 L common-rail diesel engine (peak Brake Specific Fuel Consumption (BSFC) ≈ 188 g/kWh). The scaling methodology proposed in [32] was applied to adapt this reference map to the larger 6-cylinder engine of the Isuzu truck. In particular, torque values were scaled proportional to engine displacement, assuming the same mean effective pressure for both engines, and engine speed was scaled inversely with engine stroke length (imposing equal mean piston speed for the reference and target engines). More details about the development and validation of the model can be found in a previous work of the authors [33]. The resulting engine maps are shown in Figure 2.

Figure 3 reports the results of the validation. Across the entire dataset, the predicted total fuel consumption for each trip was generally within ±5% of the measured value, with an average error of approximately 2–3%. This level of accuracy was achieved despite no explicit adjustments being made for cold-start versus hot-start differences in engine efficiency, indicating that the quasi-static map-based model effectively captured the dominant effects on fuel use.

It is noted that map-based engine models can be unreliable at very low loads (near idling) [34]. To address this, the model directly utilized experimental fuel consumption and exhaust flow

rates as constant values when the engine was at idle. In the dataset, the idle fuel flow was approximately 0.5 g/s, and the exhaust mass flow was about 0.035 kg/s (averaged across all trips). Substituting these measured idle values into the simulation ensured a more realistic behavior of the model during vehicle stops and very low engine load conditions.

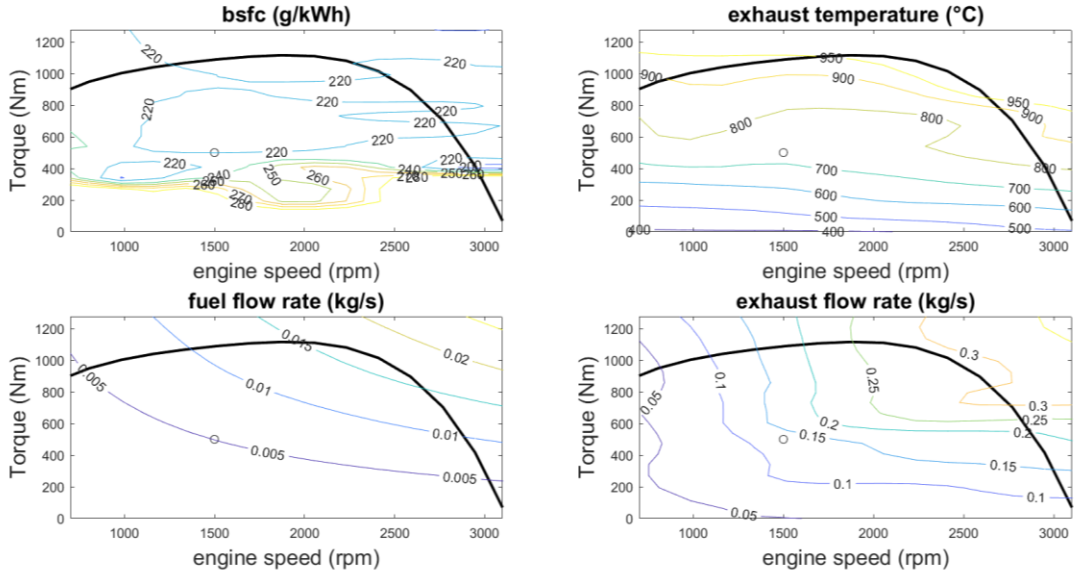

Figure 2. Maps of BSFC, exhaust temperature, fuel flow rate, and exhaust flow rate of ISUZU6HK1.

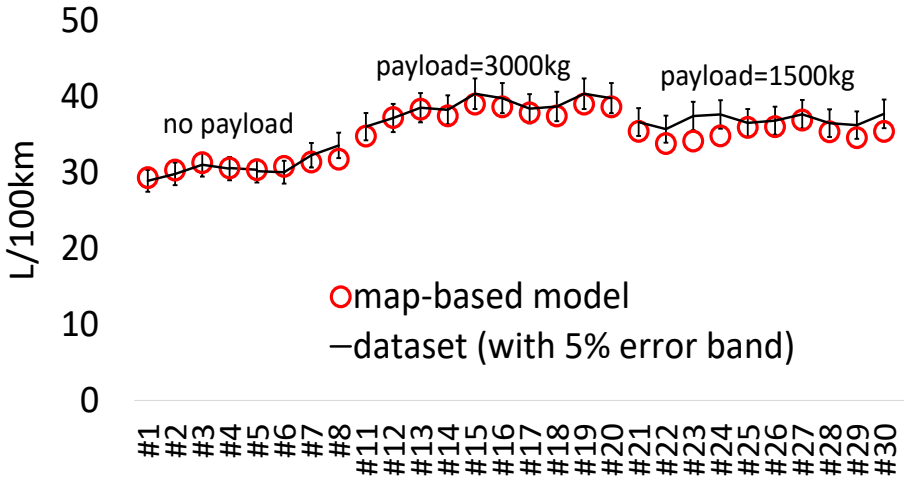

Figure 3. Validation of the map-based model for fuel consumption.

3.1 Exhaust Gas Flow and Temperature Modelling for WHR

Accurate prediction of exhaust flow rate and temperature is crucial for evaluating the WHR potential. In the developed model, the engine map provides exhaust gas conditions corresponding to the engine operating points. However, the reference map data from the Simulink model yields exhaust properties at the turbine outlet, the so-called “hot end” of the exhaust path. On the other hand, the experimental measurements were taken at the tailpipe by the PEMS, i.e., the “cold end” of the exhaust path. Using the map exhaust temperature directly would neglect heat losses along the exhaust line. Unfortunately, detailed information about the truck’s exhaust system (pipe geometry, lengths, etc.) was not available to support a first-principles thermal model of the

exhaust. Therefore, a simplified empirical approach was adopted to estimate the tailpipe exhaust temperature from the map-based (turbine-out) values.

In the absence of better data, the model calculates the exhaust temperature at the tailpipe as the map-based hot-end temperature minus 350 °C. Then, it applies a moving-average filter to dampen rapid fluctuations. The constant 350 °C offset was chosen so that the simulated tailpipe exhaust temperature for a fully warm trip matched the measured PEMS data. This value was tuned using trip #4 and then applied universally to all trips. In addition, to support the WHR analysis, an "intermediate" exhaust gas temperature was calculated as the simple average of the hot-end and cold-end values at each time step. This intermediate temperature can be interpreted as the exhaust temperature available at a midpoint in the exhaust line, e.g., at a potential WHR heat exchanger location.Using the above method, the model was able to reproduce the trends of exhaust mass flow and tailpipe temperature with reasonable fidelity. Figure 4 shows a representative example (trip #4, hot start) of the modelled exhaust mass flow rate and the estimated tailpipe temperature compared against experimental data. The exhaust flow rate prediction closely follows the measured values for all phases of the trip, and the tailpipe temperature estimation captures the overall behavior, albeit with some expected steady bias due to the fixed offset. A similar agreement was observed for other trips (for instance, trip #14, which had a higher payload and different ambient conditions, showed analogous results).

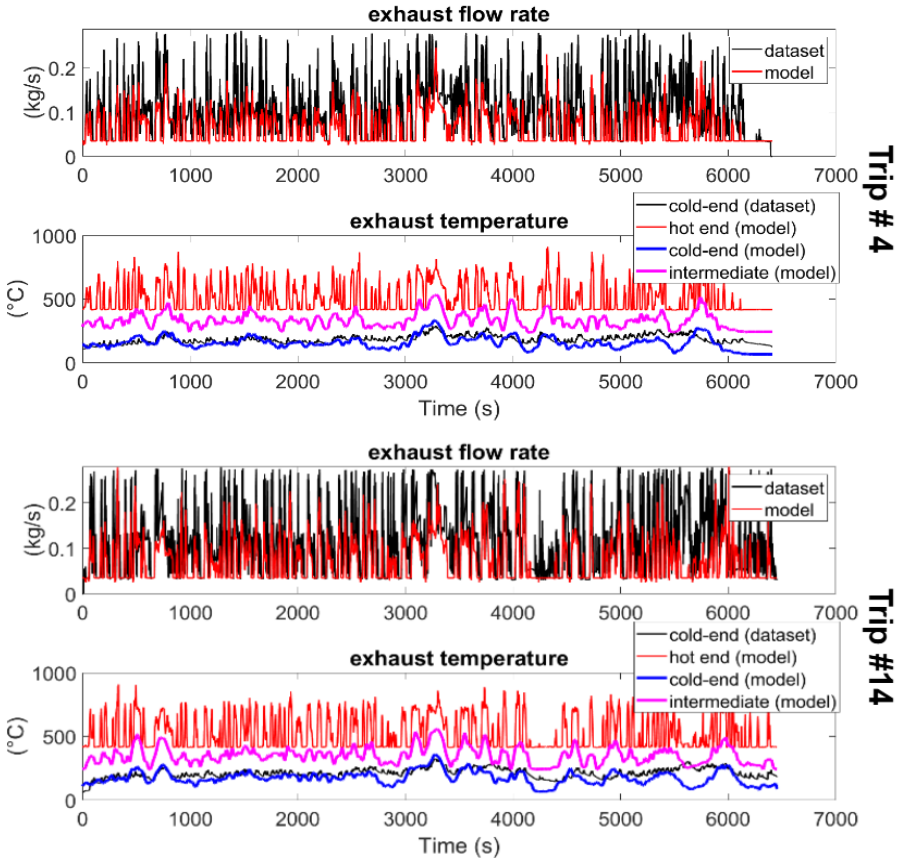

Figure 4. Validation of the proposed model in terms of exhaust flow rate (top), calibration of cold-end temperature, and estimation of intermediate temperature (bottom) on trips #4 and #14

The proposed model estimates reasonably the frequency distribution of exhaust temperature and mass flow [33]. This makes it useful for the sizing of the heat recovery system that will be

performed based on the most recurrent engine operating points. However, the plots of Figure 4 show that the dynamic behavior of the exhaust temperature, caused by the thermal inertia, is not well capture. To solve this problem and improve the prediction of fuel consumption, exhaust gas temperature, and flow rate under cold start operation, machine learning methods are being developed.

3.2 Frequency analysis

Since the engine operating conditions vary continuously in the trips, the model presented above was used to identify the most recurrent engine working points to be used for the design of the ORC. The results of the frequency analysis are reported in Figure 5, where the engine map was divided into bins of 100 rpm × 50 Nm. Each bin was then colored according to the frequency of torque and speed values in the entire data set (28 trips).

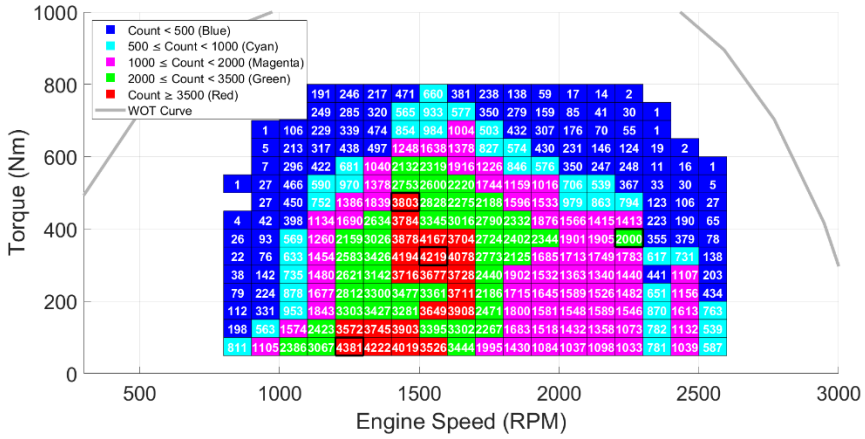

Figure 5. Results of the frequency analysis and selected modes

Note that the most recurrent engine working points (red bins) are in the middle of the plot and the medium-low speed, very low torque region. From this red region, the first three modes, as reported in Table 4, were selected. Mode 4 was chosen as the most frequent in the high-torque, high-speed region, where the engine presents higher values of exhaust gas temperature and mass flow rate, which can be suitable for sizing the ORC.

Table 4. Details of the selected engine modes

	Mode 1	**Mode 2**	**Mode 3**	**Mode 4**
Engine speed n_{ice} (rpm)	1550	1450	1250	2250
Engine torque T_{ice} (Nm)	325	475	75	375
Mechanical power P_{mech} (kW)	52.8	72.1	9.8	88.4
P_{chem} (kW)	237.1	300.1	53.0	418.1
Engine efficiency η_{ice}	0.22	0.24	0.19	0.21
Fuel flow rate $\dot{m}_{fuel}$ (g/s)	5.45	6.90	1.22	9.61
Exhaust power P_{exh}(kW)	74.2	87.9	28.7	117.4
Exhaust flow rate $\dot{m}_{exh}$ (kg/s)	0.109	0.114	0.059	0.152
Hot-end temperature T_{exh} (°C)	639.1	718.2	462.3	720.3
Cold-end temperature (°C)	289.1	368.2	112.3	370.3

In this table, mechanical power was calculated as:

$$P_{mech} = T_{ice} \cdot \frac{2\pi}{60} n_{ice} \quad (3)$$

Where n_{ice} is the engine speed in rpm while $T_{ice}$is the torque.
The chemical power of the fuel is given by:

$$P_{chem} = \dot{m}_{fuel} LHV \quad (4)$$

Where $\dot{m}_{fuel}$ is the mass flow rate from the dataset and LHV is the lower heating value of diesel fuel (43500 MJ/kg).
The engine efficiency was obtained from the BSFC map:

$$\eta_{ice} = \frac{1}{bsfc \cdot LHV} = P_{mech}/P_{chem} \quad (5)$$

The exhaust thermal power is computed as:

$$P_{exh} = \dot{m}_{exh} c_p (T_{int} - T_{amb}) \quad (6)$$

Where the mass flow rate $\dot{m}_{exh}$ of the exhaust gases (hot-end) is obtained from the engine maps, while the intermediate temperature T_{int} is calculated by the model (see Figure 4). The constant pressure specific heat of the exhaust gases, c_p, and the ambient temperature T_{amb} were assumed to be equal to 1100 J/kg.K and 20°C, respectively.

4. Preliminary sizing and off-design of the ORC

A quasi-static numerical model was developed to evaluate the performance of an ORC system for waste heat recovery. This model enables assessment of the system's energy recovery potential under design and off-design operating conditions typical of road transportation.

The model considers a plate heat exchanger for the thermal energy transfer between the exhaust gases and the organic working fluid. The thermal performance of the heat exchanger is estimated using heat transfer coefficients and heat exchange surface areas representative of hybrid engine operating conditions, based on data reported by Karellas et al [35].

After a preliminary analysis of the engine operating mode, the ORC system was sized based on the thermal energy content of the exhaust gases at mode 1. Specifically, the exhaust gas power input of modes 1-4 was selected in turn to represent steady-state operation at nominal engine load, and the other modes were used to pre-analyze the off-design behavior. The intermediate temperature was used as input, together with the exhaust mass flow rate. The electric efficiency of the ORC was calculated through a code already developed in previous work [36]. The model incorporates numerical stability checks and enforces physical constraints, such as maintaining a minimum operating pressure of the working fluid, to ensure robustness and consistency with real operating conditions.

The ORC configuration is without internal heat regeneration to limit overweighting. To characterize system performance under partial-load conditions, which are critical for vehicle operation, the model employs normalized efficiency curves derived from the literature [37]. These curves have been widely validated and show limited sensitivity to the specific size of the ORC system, allowing reliable off-design performance estimation. The flowchart of the plant is shown

in Figure 6, along with the main specifications of the plant. The valve system shown in the ORC scheme is designed to allow the ORC to operate safely, divert exhaust gases when the temperature is too high, and enable flow rate regulation.

The overall performances of the WHR system were then calculated over the whole dataset, including only ORC temperatures within the operating range to avoid deterioration of the organic fluid. The performance indexes used for the preliminary design of the ORC are plant efficiency and the Utilization Factor (UF), which indicates how much of the trip time is effectively utilized at nominal-equivalent power. If UF remains below 1, the system often operates under partial load, highlighting the importance of matching ORC size to real driving conditions. The overall efficiency was found to be 6.57%, accounting for all trips and filtered temperature values.

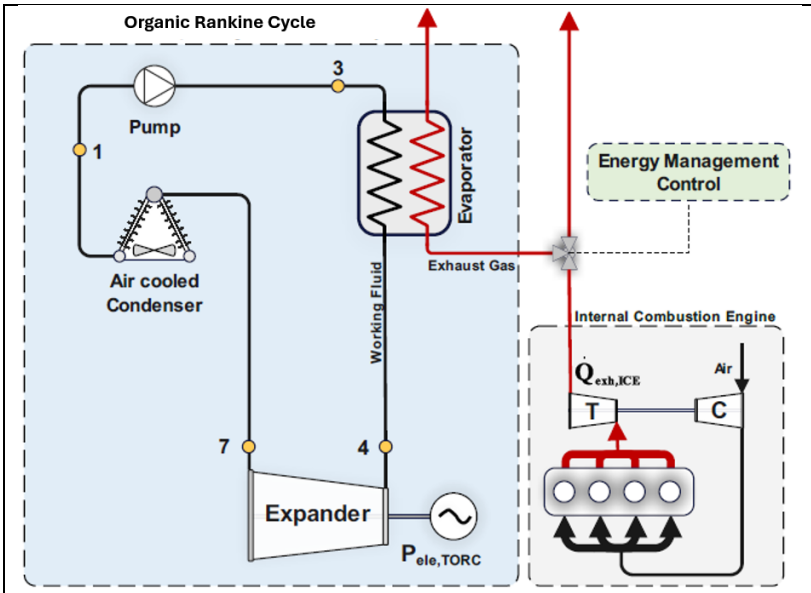

Operating fluid	R245F
Type of expander	Scroll
Condenser pressure	1.78bar
Evaporator pressure	58.4 bar
Expander inlet temperature	250°C
Average efficiency	6.6%
Utilization factor	41.9%
Average electric power	2kW
Estimated weight of heat exchanger	17.5kg

Figure 6. Flow chart and specifications of the ORC plant

To estimate the weight of an ORC system suitable for the application discussed in the paper, the authors referred to a study by Pili et al. [38], which investigates various working fluids under typical exhaust gas conditions encountered in HDVs on highways. The study focuses on simplified ORC configurations without recuperation, optimized for minimal weight, and provides corresponding Power-to-Weight (PTW) ratios. Pili et al. consider only the weight of the heat exchanger core, as it represents the most significant contribution to the system's overall mass [39]. The reported PTW values range from 26 to 77 W/kg, depending on the specific setup; the wide range is primarily influenced by the choice of working fluid. These findings highlight the significant impact of fluid selection and system design on the total weight, a key factor for mobile applications such as automotive waste heat recovery.

A sensitivity analysis and a multi-objective optimization of the whole powertrain comprehensive of ORC, heat exchanger, and hybrid electric path, will be performed in the continuation of the project.

5. Sizing and managing the hybrid electric power system

A parallel architecture was selected for the preliminary analysis of the integrated hybrid-ORC powertrain and to compare it with a series-parallel configuration in the continuation of the project. The simplified scheme is shown in Figure 7.

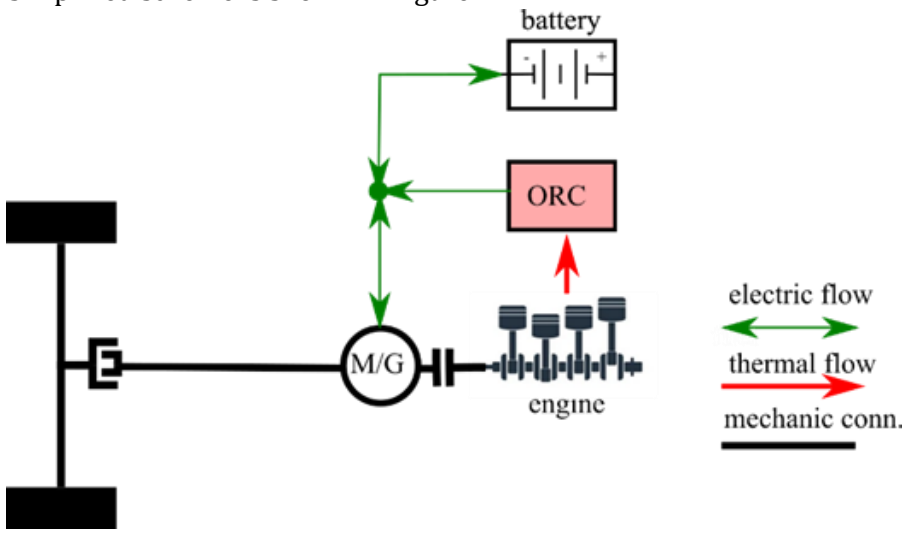

Figure 7. Simplified scheme of the proposed architecture.

For this preliminary analysis, the authors made several hypotheses and simplifications. The analysis focuses on trip #14, which falls within the class of trips carrying a 3,000-kilogram payload. The additional mass of the hybrid powertrain, with or without the ORC system, is assumed to be negligible compared to the combined weight of the payload and the truck itself. As a result, the additional mass of the powertrain does not increase the power demand—it simply reduces the payload capacity.

The auxiliary power demand of 2 kilowatts is covered either by the battery in the hybrid configuration without WHR or by the ORC system in the configuration that includes it, based on the results of the preliminary sizing of the ORC (Figure 6).

The engine is operated at a constant power setpoint $P_{ICE}d$, when the vehicle is in traction, and it is turned off during stops and braking phases. The engine speed at each time step remains the same as in the original configuration, assuming the same gearbox and shifting strategy. This strategy will be henceforth referred to as CPEMS (Constant Power Energy Management Strategy).

More specifically, the engine power at time step "i" is calculated as:

$$P_{ICE}(i) = \begin{cases} 0 & if \;\; P_w(i) \leq 0 \\ P_{ICE}d & if \; P_w(i) > 0 \end{cases} \quad (7)$$

A sensitivity analysis performed in a previous work by some of the authors [33] revealed that $P_{ICE}d = 50\ kW$ is a good compromise between fuel consumption, battery mass, and average exhaust temperature. At this stage, we only consider hot-start engine operation.

The battery-electric machine driveline is used to balance the difference between the required power and what the engine provides. At each time step, the power of the battery $\mathrm{P_{batt}}(i)$ is calculated as:

$$\mathrm{P_{batt}}(i) = P_{EM}(i)/\eta_{EM}^{\gamma} \quad (8)$$

Where $P_{EM}(i) = P_w(i) - P_{ICE}(i)$ is the mechanical power of the electric machine, and γ is equal to 1 or -1 when the electric machine works as a motor or generator, respectively. A constant efficiency of 90 percent is considered for the electric machine in both modes.

For sizing the battery, two approaches were employed. In the first case, the battery is used as an energy buffer. The energy and maximum battery power requirements of trip #14 are the inputs for sizing the battery using the procedure described in [55]. We assumed a Depth of Discharge of 70 percent, a gravimetric energy density of 150 watt-hours per kilogram, and a discharge C-rate of 15C. Regenerative braking power is limited to 7 kilowatts in order to preserve battery health.

In the second sizing approach (charge depleting or plug-in). The battery was sized with the goal of achieving the battery depleting in a whole working day and charging the battery overnight. The daily working cycle was obtained by composing some trips as in Table 5. The engine's contribution to propulsive power is decided by a Fuzzy Logic Energy Management Strategy (FLEMS).

Table 5. Daily working cycle adopted for the charge-depleting strategy

Daily working cycle	Speed profile	Payload
Section 1	Trip #4	0 kg
Section 2	Trip #14	3000 kg
Section 3	Trip #23	1500 kg
Section 4	Trip #4	0 kg

5.1 Energy management strategy (plug-in version)

Fuzzy logics were chosen for energy management due to their ability to smooth changes in engine setpoints and their ease of online applicability, which is guaranteed by the low required computational time. The inputs used for the fuzzy logic are the battery SOC, the vehicle speed, and the acceleration. The output is the engine utilization u defined as:

$$u(i) = P_{ICE}(i)/P_w(i) \quad (9)$$

The membership functions adopted in this investigation are shown in Figure 8. They were derived empirically with a trial-and-error approach, but will be optimized in the continuation of the project.

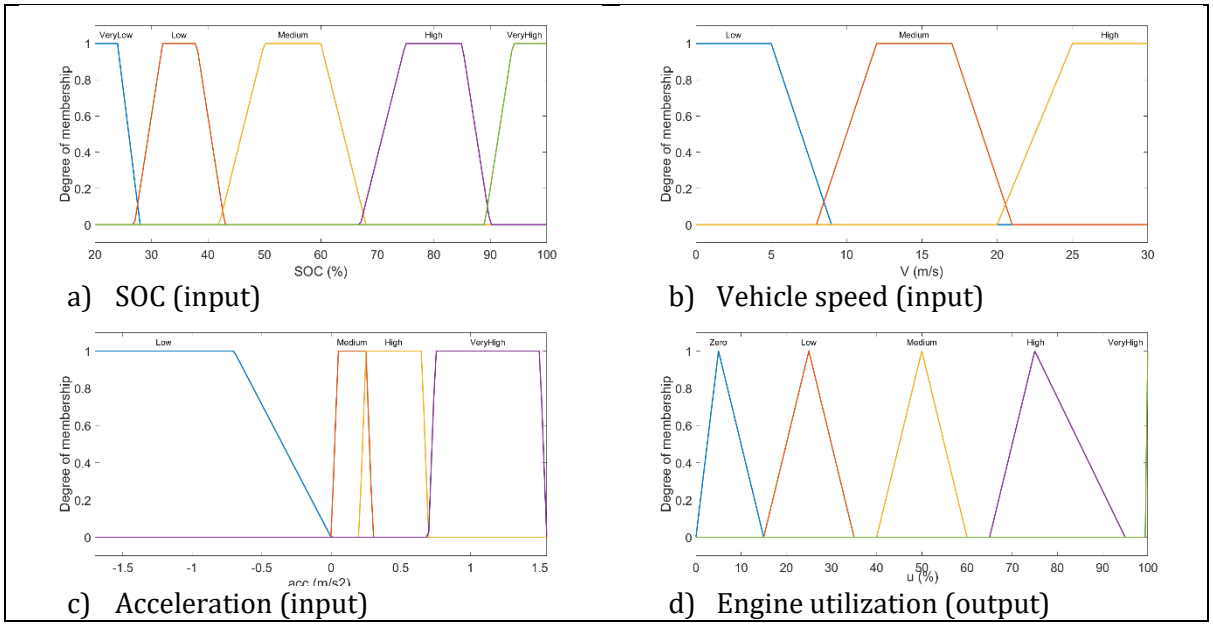

Figure 8. Membership functions for the inputs and outputs of the fuzzy logic

The inference engine is based on the rules reported in Table 6. From those rules, a 3D map of engine contribution is obtained and implemented.

Table 6. Rules of the fuzzy logic energy management strategy

Speed	Acceleration	SOC	u	Speed	Acceleration	SOC	u
Low	Low	Verylow	Zero	Medium	High	Verylow	Veryhigh
Low	Low	Low	Zero	Medium	High	Low	High
Low	Low	Medium	Zero	Medium	High	Medium	Medium
Low	Low	High	Zero	Medium	High	High	Low
Low	Low	Veryhigh	Zero	Medium	High	Veryhigh	Zero
Low	Medium	Verylow	Veryhigh	Medium	Veryhigh	Verylow	Veryhigh
Low	Medium	Low	High	Medium	Veryhigh	Low	High
Low	Medium	Medium	High	Medium	Veryhigh	Medium	Medium
Low	Medium	High	Medium	Medium	Veryhigh	High	Medium
Low	Medium	Veryhigh	Zero	Medium	Veryhigh	Veryhigh	Zero
Low	High	Verylow	Veryhigh	High	Low	Verylow	Zero
Low	High	Low	High	High	Low	Low	Zero
Low	High	Medium	High	High	Low	Medium	Zero
Low	High	High	Medium	High	Low	High	Zero
Low	High	Veryhigh	Zero	High	Low	Veryhigh	Zero
Low	Veryhigh	Verylow	Veryhigh	High	Medium	Verylow	Veryhigh
Low	Veryhigh	Low	High	High	Medium	Low	Veryhigh
Low	Veryhigh	Medium	Low	High	Medium	Medium	Veryhigh
Low	Veryhigh	High	Zero	High	Medium	High	Veryhigh
Low	Veryhigh	Veryhigh	Zero	High	Medium	Veryhigh	Zero
Medium	Low	Verylow	Zero	High	High	Verylow	Veryhigh
Medium	Low	Low	Zero	High	High	Low	High
Medium	Low	Medium	Zero	High	High	Medium	High
Medium	Low	High	Zero	High	High	High	Medium
Medium	Low	Veryhigh	Zero	High	High	Veryhigh	Zero
Medium	Medium	Verylow	Veryhigh	High	Veryhigh	Verylow	Veryhigh
Medium	Medium	Low	High	High	Veryhigh	Low	High
Medium	Medium	Medium	High	High	Veryhigh	Medium	High
Medium	Medium	High	Medium	High	Veryhigh	High	Medium
Medium	Medium	Veryhigh	Zero	High	Veryhigh	Veryhigh	Zero

6. Results

The distributions of the engine working points obtained in the hybrid configurations for trip #14 are reported in Figure 9. Note that for the CPEMS strategy (Figure 9a), the points are located on the constant power line (50 kW). The high-frequency region corresponds to higher values of engine speed and torque than those considered for sizing the ORC (Mode 1 of Table 4). This means that the ORC should be redesigned on the basis of the new engine working points. In the case of the fuzzy-logic strategy (Figure 9b), the engine working points are mostly in the medium-speed, low-torque region. This indicates the possibility of downsizing the engine to improve fuel consumption. In both cases, the need to synergically optimize the design and energy management of the whole powertrain inclusive of hybridization and waste-heat recovery is evident.

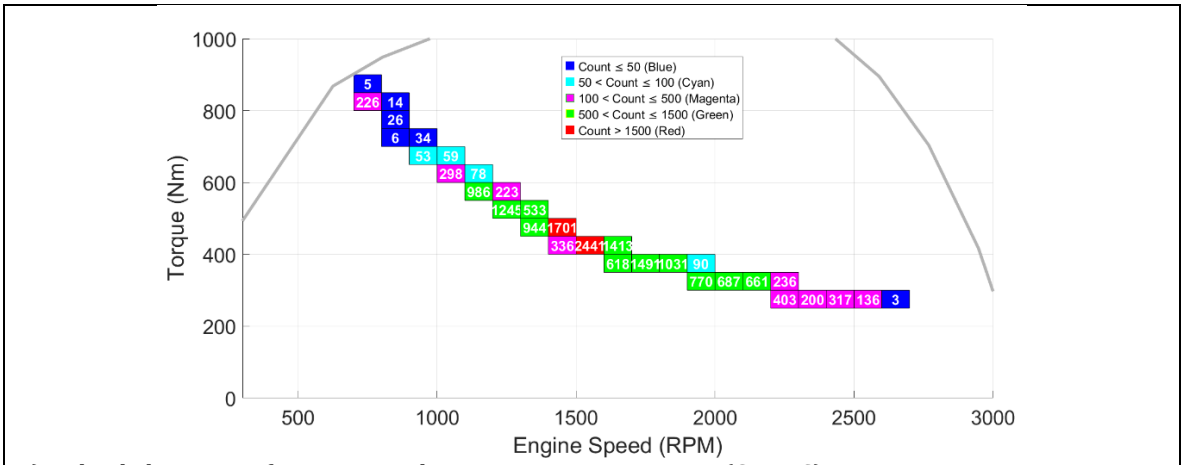

a) Hybrid electric configuration with constant power strategy (CPEMS)

b) Hybrid electric configuration with the fuzzy-logic strategy (FLEMS)

Figure 9. Frequency distribution of the engine working points with the proposed strategies (trip #14)

Table 7 presents the values of fuel consumption and battery size for the original configuration, as well as for the configurations with hybridization and WHR, both together and separately.

These results indicate that integrating an ORC alone can reduce fuel consumption by approximately 3.5%, lowering it from 37.5 to 36.2 liters per 100 kilometers. However, this improvement comes with a trade-off: the available thermal power is reduced due to decreases in both average temperature and mass flow rate, a consequence of the engine operating at a lower

average load. This highlights the importance of finding the right balance, as ORC systems efficiently recover waste heat; however, their additional weight and volume can negatively impact vehicle load capacity and overall efficiency. These physical constraints are also critical in determining the system's capital cost.

Hybridization without the ORC leads to a more significant fuel reduction of 14.7% (from 37.5 to 32.0 liters/100 km) and increases the average exhaust temperature by 22.7%. Additionally, the exhaust temperature becomes more stable, as evidenced by a decrease in its standard deviation. This improvement results from the near alignment of the constant power and constant exhaust temperature curves on the engine map. Since the engine is shut off during stops and braking, the average mass flow rate decreases, even though the exhaust flow remains nearly constant when the engine is active. It is important to note that a rise in exhaust temperature does not always enhance waste heat recovery, as excessively high temperatures may exceed the operational limits of the organic fluid or the PCM. These challenges will be addressed in the next phase of the study through the development of a realistic and optimized energy management strategy. This will include the integration of a PCM-based heat exchanger and refined powertrain sizing, encompassing hybridization, PCM, and WHR systems.

Adding the ORC system does not alter the engine's operating point but does reduce the required battery mass by 16% (−17 kg). However, this benefit is offset by the additional mass of the ORC system.

With the FLEMS approach, the battery is much larger than in the CPEMS approach (76 vs 15.0 kWh) and is slowly discharged throughout the whole working day, as shown in Figure 10. This results in a significant reduction in daily fuel consumption, which is 32% lower than in the original configuration. The strategy will be refined in the continuation of the project to maximize waste heat recovery and minimize cold-start operations of the engine.

Moreover, AI-based techniques will be explored for predicting exhaust temperatures and additional fuel consumption under cold-start conditions. Further aspects to be addressed include the role of aftertreatment systems in modern diesel engines, their exhaust temperature requirements, and the impact of the heat exchanger on backpressure.

Table 7. Potentiality of hybridization and WHR calculated for trip #14 (payload: 3000 kg).

Configuration	**Energy management strategy**	**Fuel consumption** (L/100km)	**Battery cell**	**Battery size** (kWh)
Original	-	37.5	-	-
Original + ORC	CPEMS	36.2	-	-
Hybrid electric	CPEMS	32.0	Generic lithium-ion	15.5
Hybrid electric with ORC	CPEMS	32.0	Generic lithium-ion	12.9
Hybrid electric + ORC	FLEMS	25.5	High Rate LiFePo4 (4Ah, 3.2V, 5C)	76

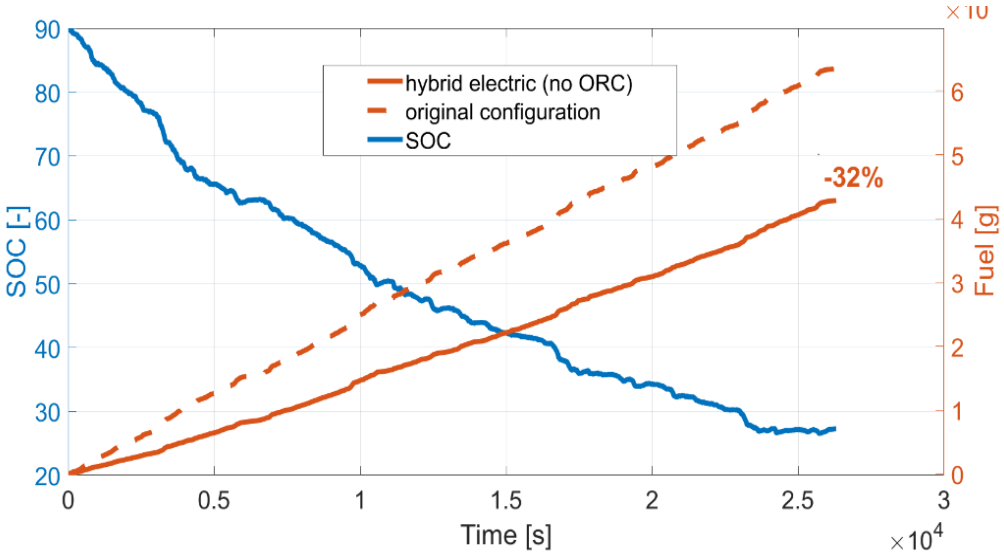

Figure 10. Battery SOC and cumulative fuel consumption (whole working day)

7. Conclusions and future developments

This investigation proposes the integration of hybridization and waste heat reduction to help diesel truck to cut HDV emissions (CO_2 and pollutants) in line with Euro VII, EPA, and China VI/VII requirements. In particular, sizing methodologies for the ORC and the Hybrid electric drive are proposed and compared on a reference truck (ISUZU FTR850).

A map-based quasi-stationary approach was adopted for the simulation of the original powertrain and validated using a large dataset of driving conditions. The ORC system was sized and modeled for part-load operation, and a sensitivity analysis revealed that it could consistently supply the auxiliary power demand, estimated at around 2 kW.

A preliminary sizing based on a constant engine power setpoint demonstrated a 15% reduction in fuel consumption. Additionally, a charge-depleting fuzzy-logic control strategy applied over an 8-hour working cycle indicated an even greater potential benefit, with a 32% reduction in fuel use, although this result still requires further validation.

The analysis of the most recurrent engine points in the original and hybrid configurations with the two energy management strategies stressed the need for a synergic optimization of the design and management of the proposed powertrain that will be the main future development of the projects, together with improvements to the several submodels.

8. Funding and acknowledgments

We acknowledge financial support under the National Recovery and Resilience Plan (NRRP), Mission 4, Component 2, Investment 1.1, Call for tender No. 1409 published on 14.9.2022 by the Italian Ministry of University and Research (MUR), funded by the European Union – NextGenerationEU – Project Title IRIDESCENT – P2022YB8HY CUP F53D23009880001 - Grant Assignment Decree No. 5 adopted on 01/09/2023 by the Italian Ministry of University and Research (MUR).

9. References

[1] M. Shane, "Tracking Trucks and Buses," IEA. Accessed: Apr. 15, 2025. [Online]. Available: https://www.iea.org/energy-system/transport/trucks-and-buses

[2] C. Cunanan, M.-K. Tran, Y. Lee, S. Kwok, V. Leung, and M. Fowler, "A Review of Heavy-Duty Vehicle Powertrain Technologies: Diesel Engine Vehicles, Battery Electric Vehicles, and Hydrogen Fuel Cell Electric Vehicles," *Clean Technol.*, vol. 3, no. 2, Art. no. 2, Jun. 2021, doi: 10.3390/cleantechnol3020028.

[3] "Euro VI trucks still don't meet emission limits on the road," Oct. 2021. [Online]. Available: https://www.transportenvironment.org/uploads/files/2021_11_Euro_VII_HD_policy_paper_2021.pdf#:~:text=levels%2C%20especially%20since%20high%20cold,limit%20from%20the%20175%20mg%2FkWh

[4] Z. C. Samaras *et al.*, "A European Regulatory Perspective towards a Euro 7 Proposal", Accessed: Apr. 15, 2025. [Online]. Available: https://www.sae.org/publications/technical-papers/content/2022-37-0032/

[5] L. Xu, F. Zhao, H. Wei, P. Zhao, W. Qian, and M. Qian, "The Development of a Zeolite-Based Cold-Start Catalyst (CSC) for a Conventional China 6b Vehicle in Meeting the Next More Stringent Chinese Vehicle Emission Standards," SAE International, Warrendale, PA, SAE Technical Paper. Accessed: Apr. 15, 2025. [Online]. Available: https://www.sae.org/publications/technical-papers/content/2023-01-0233/

[6] Z. Reggie, "An examination of China 7 emissions regulations," F&L Asia. Accessed: Apr. 15, 2025. [Online]. Available: https://www.fuelsandlubes.com/fli-article/an-examination-of-china-7-emissions-regulations/

[7] Yihao Xie, "U.S. heavy-duty vehicle NOX standards: Updates to emission limits, testing requirements, and compliance procedures," © 2023 INTERNATIONAL COUNCIL ON CLEAN TRANSPORTATION, Jul. 2023. [Online]. Available: https://theicct.org/wp-content/uploads/2023/07/us-nox-standards-update-jul23.pdf#:~:text=,to%20the%20current%202010

[8] D. Mohr, T. Shipp, and X. Lu, "The Thermodynamic Design, Analysis and Test of Cummins' Supertruck 2 50% Brake Thermal Efficiency Engine System," SAE International, Warrendale, PA, SAE Technical Paper. Accessed: Apr. 15, 2025. [Online]. Available: https://www.sae.org/publications/technical-papers/content/2019-01-0247/

[9] "Experimental analysis of the global energy balance in a DI diesel engine | Request PDF," *ResearchGate*, Oct. 2024, doi: 10.1016/j.applthermaleng.2015.06.005.

[10] B. Xu, D. Rathod, A. Yebi, Z. Filipi, S. Onori, and M. Hoffman, "A comprehensive review of organic rankine cycle waste heat r", Accessed: Apr. 15, 2025. [Online]. Available: https://ideas.repec.org//a/eee/rensus/v107y2019icp145-170.html

[11] A. Mahmoudzadeh Andwari, A. Pesiridis, A. Karvountzis-Kontakiotis, and V. Esfahanian, "Hybrid Electric Vehicle Performance with Organic Rankine Cycle Waste Heat Recovery System," *Appl. Sci.*, vol. 7, no. 5, Art. no. 5, Apr. 2017, doi: 10.3390/app7050437.

[12] C. Yang and Y. Li, "Fuel-saving performance and main losses of an organic-Rankine-cycle-based exhaust heat recovery system in heavy truck application scenarios," *Appl. Therm. Eng.*, vol. 193, p. 117025, Jul. 2021, doi: 10.1016/j.applthermaleng.2021.117025.

[13] S. Broekaert, T. Grigoratos, D. Savvidis, and G. Fontaras, "Assessment of waste heat recovery for heavy-duty vehicles during on-road operation," *Appl. Therm. Eng.*, vol. 191, p. 116891, Jun. 2021, doi: 10.1016/j.applthermaleng.2021.116891.

[14] S. Thantla, J. Aspfors, M. Ghanbarpour, and J. Fridh, "Performance analysis of a dual-loop organic Rankine cycle system for waste heat recovery from engine coolant and exhaust of a heavy-duty truck," *Appl. Therm. Eng.*, vol. 219, p. 119203, Jan. 2023, doi: 10.1016/j.applthermaleng.2022.119203.

[15] C. Wang, F. Yang, H. Zhang, R. Zhao, and Y. Xu, "Energy recovery efficiency analysis of organic Rankine cycle system in vehicle engine under different road conditions," *Energy Convers. Manag.*, vol. 223, p. 113317, Nov. 2020, doi: 10.1016/j.enconman.2020.113317.

[16] M. Zhao, M. Wei, G. Tian, and P. Song, "Simulation of effects of ORC system installation on heavy-duty truck," *Appl. Therm. Eng.*, vol. 128, pp. 1322–1330, Jan. 2018, doi: 10.1016/j.applthermaleng.2017.09.114.

[17] V. P. and D. Deshmukh, "A comprehensive review of waste heat recovery from a diesel engine using organic Rankine cycle," *Energy Rep.*, vol. 7, pp. 3951–3970, Nov. 2021, doi: 10.1016/j.egyr.2021.06.081.

[18] C. Wieland, C. Schifflechner, F. Dawo, M. Astolfi "The organic Rankine cycle power systems market: Recent developments and future perspectives,". *Applied thermal engineering*. Apr. 2023 1;224:119980, doi:10.1016/j.applthermaleng.2023.119980

[19] Z. Li *et al.*, "Experimental investigations on dynamic performance of organic Rankine cycle integrated with latent thermal energy storage under transient engine conditions," *Energy*, vol. 246, p. 123413, May 2022, doi: 10.1016/j.energy.2022.123413.

[20] X. Yu, Z. Li, Y. Lu, R. Huang, and A. P. Roskilly, "Investigation of organic Rankine cycle integrated with double latent thermal energy storage for engine waste heat recovery," *Energy*, vol. 170, pp. 1098–1112, Mar. 2019, doi: 10.1016/j.energy.2018.12.196.

[21] C. Cunanan, M.-K. Tran, Y. Lee, S. Kwok, V. Leung, and M. Fowler, "A Review of Heavy-Duty Vehicle Powertrain Technologies: Diesel Engine Vehicles, Battery Electric Vehicles, and Hydrogen Fuel Cell Electric Vehicles," *Clean Technol.*, vol. 3, no. 2, Art. no. 2, Jun. 2021, doi: 10.3390/cleantechnol3020028.

[22] A. Mahmoudzadeh Andwari, A. Pesiridis, A. Karvountzis-Kontakiotis, and V. Esfahanian, "Hybrid Electric Vehicle Performance with Organic Rankine Cycle Waste Heat Recovery System," *Appl. Sci.*, vol. 7, no. 5, Art. no. 5, Apr. 2017, doi: 10.3390/app7050437.

[23] E. Nivolianiti, Y. L. Karnavas, and J.-F. Charpentier, "Fuzzy Logic-Based Energy Management Strategy for Hybrid Fuel Cell Electric Ship Power and Propulsion System," *J. Mar. Sci. Eng.*, vol. 12, no. 10, Art. no. 10, Oct. 2024, doi: 10.3390/jmse12101813.

[24] A. Mazouzi, N. Hadroug, W. Alayed, A. Hafaifa, A. Iratni, and A. Kouzou, "Comprehensive optimization of fuzzy logic-based energy management system for fuel-cell hybrid electric vehicle using genetic algorithm," *Int. J. Hydrog. Energy*, vol. 81, pp. 889–905, Sep. 2024, doi: 10.1016/j.ijhydene.2024.07.237.

[25] H. Yu, F. Castelli-Dezza, F. Cheli, X. Tang, X. Hu, and X. Lin, "Dimensioning and Power Management of Hybrid Energy Storage Systems for Electric Vehicles with Multiple Optimization Criteria," *IEEE Trans. Power Electron.*, vol. 36, no. 5, pp. 5545–5556, May 2021, doi: 10.1109/TPEL.2020.3030822.

[26] J. W. Joubert and R. J. Gräbe, "Real driving emissions data: Isuzu FTR850 AMT," *Data Brief*, vol. 41, p. 107975, Apr. 2022, doi: 10.1016/j.dib.2022.107975.

[27] "Isuzu Engines," Isuzu Diesel Engines. Accessed: Mar. 19, 2025. [Online]. Available: https://www.isuzuengines.com/

[28] T. Donateo, P. Cutuli, N. Vilotta, A. Algieri, and P. Morrone, "Analysis of the Heat Content of Exhaust Gases from a Heavy-Duty Diesel Engine under Real-world Driving Conditions and Cold Start Operation," *J. Phys. Conf. Ser.*, vol. 2893, no. 1, p. 012103, Nov. 2024, doi: 10.1088/1742-6596/2893/1/012103.

[29] M. Villani, S. Lombardi, and L. Tribioli, "Performance Evaluation of a Heavy-Duty Diesel Truck Retrofitted with Waste Heat Recovery and Hybrid Electric Systems," *SAE Int. J. Electrified Veh.*, vol. 9, no. 1, pp. 41–60, 2020.

[30] M. Hammache, M. Michaelian, and F. Browand, "Aerodynamic forces on truck models, including two trucks in tandem," 2001, Accessed: Mar. 19, 2025. [Online]. Available: https://escholarship.org/content/qt6jr154q9/qt6jr154q9.pdf

[31] G. Arts, "Analysis and synthesis of hybrid truck energy management," 2007. Accessed: Nov. 07, 2024. [Online]. Available: https://www.semanticscholar.org/paper/Analysis-and-synthesis-of-hybrid-truck-energy-Arts/b6502975fe88255122d117622e19d540c9178893

[32] M. Sorrentino, F. Mauramati, I. Arsie, A. Cricchio, C. Pianese, and W. Nesci, "Application of Willans Line Method for Internal Combustion Engines Scalability towards the Design and Optimization of Eco-Innovation Solutions," SAE International, Warrendale, PA, SAE Technical Paper 2015-24–2397, Sep. 2015. doi: 10.4271/2015-24-2397.

[33] T. Donateo, T. Mujahid, P. Morrone, and A. Algieri, "Analysis and simulation of fuel consumption and emissions in a Heavy-Duty Diesel truck under real-world driving conditions for hybridization and waste heat recovery," *SAE Technical Paper* 2025-24-0096, 2025, doi: 10.4271/2025-24-0096.

[34] L. Guzzella and A. Sciarretta, *Vehicle Propulsion Systems: Introduction to Modeling and Optimization*. Berlin, Heidelberg: Springer, 2013. doi: 10.1007/978-3-642-35913-2.

[35] S. Karellas, A. Schuster, and A.-D. Leontaritis, "Influence of supercritical ORC parameters on plate heat exchanger design," *Appl. Therm. Eng.*, vol. 33–34, pp. 70–76, Feb. 2012, doi: 10.1016/j.applthermaleng.2011.09.013.

[36] P. Morrone, A. Algieri, and T. Castiglione, "Hybridisation of biomass and concentrated solar power systems in transcritical organic Rankine cycles: A micro combined heat and power application," *Energy Convers. Manag.*, vol. 180, pp. 757–768, Jan. 2019, doi: 10.1016/j.enconman.2018.11.029.

[37] M. Jiménez-Arreola, R. Pili, F. Dal Magro, C. Wieland, S. Rajoo, and A. Romagnoli, "Thermal power fluctuations in waste heat to power systems: An overview on the challenges and current solutions," *Appl. Therm. Eng.*, vol. 134, pp. 576–584, Apr. 2018, doi: 10.1016/j.applthermaleng.2018.02.033.

[38] R. Pili, J. D. Castro Pastrana, A. Romagnoli, H. Spliethoff, and C. Wieland, "Working Fluid Selection and Optimal Power-to-Weight Ratio for ORC in Long-Haul Trucks," *Energy Procedia*, vol. 129, pp. 754–761, Sep. 2017, doi: 10.1016/j.egypro.2017.09.116.

[39] W. Lang, P. Colonna, and R. Almbauer, "Assessment of Waste Heat Recovery From a Heavy-Duty Truck Engine by Means of an ORC Turbogenerator," *J. Eng. Gas Turbines Power*, vol. 135, no. 042313, Mar. 2013, doi: 10.1115/1.4023123.